Journal of Intelligent and Robotic Systems **14**: 105–130, 1995.

19

Calculation of Repeatable Control Strategies for Kinematically Redundant Manipulators

RODNEY G. ROBERTS* and ANTHONY A. MACIEJEWSKI
School of Electrical Engineering, Purdue University
West Lafayette, IN 47907, U.S.A. e-mail: maciejew@ecn.purdue.edu
**Present address: Department of Electrical Engineering*
FAMU/FSU College of Engineering, Florida State University
Tallahassee FL 32316-2175. e-mail: rroberts@eng.fsu.edu

(Received: 28 December 1993)

Abstract. A kinematically redundant manipulator is a robotic system that has more than the minimum number of degrees of freedom that are required for a specified task. Due to the additional freedom, control strategies may yield solutions which are not repeatable in the sense that the manipulator may not return to its initial joint configuration for closed end-effector paths. This paper compares two methods for choosing repeatable control strategies which minimize their distance from a nonrepeatable inverse with desirable properties. The first method minimizes the integral norm of the difference of the desired inverse and a repeatable inverse while the second method minimizes the distance of the null vectors associated with the desired and the repeatable inverses. It is then shown how the two techniques can be combined in order to obtain the advantages of both methods. As an illustrative example the pseudoinverse is approximated in a region of the joint space for a seven-degree-of-freedom manipulator.

Key words. Kinematically redundant, repeatability, pseudoinverse.

1. Introduction

A robotic system can be described by its kinematic equation which relates the set of joint values of the manipulator to the position and orientation of the end effector in the workspace. If the location of the end-effector is specified as an m-dimensional vector $\mathbf{x}$ then the kinematic equation can be written as

$$\mathbf{x} = \mathbf{f}(\theta) \tag{1}$$

where $\mathbf{f}$ is a smooth vector function and where θ is an n-dimensional vector of the joint variables. One of the popular techniques for controlling a manipulator is resolved motion rate control which calculates the joint velocities from the joint configuration and desired end-effector velocity. The underlying equation is the Jacobian equation which, for the positional component, can be found by differentiating (1) to obtain

$$\dot{\mathbf{x}} = J\dot{\theta} \tag{2}$$

where $\dot{\mathbf{x}}$ is the desired end-effector velocity. The chief advantage of using the Jacobian for the motion control of a manipulator is that the Jacobian is a linear relationship between the joint velocities and the end-effector velocities. At each point θ, J is an $m \times n$ matrix.

Kinematically redundant manipulators are robotic systems which possess more degrees of freedom than are required for a specified task so that $m < n$. This work will only consider the case of one degree of redundancy, i.e. when $n = m + 1$. There are an infinite number of control strategies for redundant manipulators so that one can take advantage of this freedom by choosing a control strategy which will optimize some particular criterion. This work will consider generalized inverse strategies of the form

$$\dot{\theta} = G\dot{\mathbf{x}} \tag{3}$$

where G satisfies $JG = I$ for nonsingular configurations. The elements of G are functions of the joint configuration. This strategy may be chosen to locally minimize a given criterion function such as the least-squares minimum norm criterion on the joint velocities as in the case of the pseudoinverse solution

$$\dot{\theta} = J^{+}\dot{\mathbf{x}} \tag{4}$$

where J^{+} is the Moore–Penrose pseudoinverse of J. This control strategy locally minimizes the joint velocities of the manipulator subject to moving the end-effector along a specified trajectory. Also popular in the robotics literature are weighted pseudoinverse solutions which locally minimize $\dot{\theta}^T Q \dot{\theta}$ for some positive definite weighting matrix Q. Since this work only considers manipulators with a single degree of redundancy, the generalized inverses G have the form

$$G = J^{+} + \hat{\mathbf{n}}_J \mathbf{w}^T \tag{5}$$

where $\hat{\mathbf{n}}_J$ is a unit length null vector of J and where $\mathbf{w}$ uniquely determines G. This follows from the fact that $J(G - J^{+}) = \mathbf{0}$ [9].

Due to the additional freedom afforded to kinematically redundant manipulators, control strategies such as (3) may not be repeatable in the sense that closed trajectories in the work space are not necessarily mapped to closed trajectories in the joint space so that for cyclic tasks the manipulator will not necessarily return to its starting configuration. Klein and Huang [7] give a mathematical proof of this for the pseudoinverse control of a planar 3R manipulator. An elegant method of identifying control strategies which are repeatable is presented in a paper by Shamir and Yomdin [13]. This method determines repeatability by checking whether the Lie bracket of any two columns of the inverse is in the column space of G.

This work focuses on the generation of repeatable control strategies that are as close as possible to some desirable, but not repeatable, control. It will only consider inverse kinematics and not the dynamic aspects of the complete control problem [5]. The remainder of this article is arranged as follows. In Section 2, two optimal repeatable strategies are presented. A comparison of these two strategies is discussed in Section 3 using a simple manipulator as an illustrative example. Section 4 illustrates how the two techniques can be combined by using information obtained from one technique to guide the calculation of an optimal repeatable strategy by the other technique. This procedure is demonstrated for both a simple example as well as for a seven-degree-of-freedom manipulator. Simulation results illustrating the efficacy of these techniques are presented in Section 5 followed by the conclusions of this work in the final section.

2. Two Optimal Repeatable Control Strategies

In order to choose an optimal repeatable control strategy it is necessary to characterize those strategies which are repeatable in terms of the desired generalized inverse G_d and a null space component. This will be done by considering the corresponding augmented Jacobian as was done in [9]. At nonsingular configurations any generalized inverse G can be calculated by inverting an augmented Jacobian of the form

$$J_{\mathbf{v}} = \begin{bmatrix} J \\ \cdots \\ \mathbf{v}^T \end{bmatrix} \tag{6}$$

where $\mathbf{v}$ is a null vector of G^T. The corresponding control strategy is found by taking the first $n - 1$ columns of the inverse of $J_{\mathbf{v}}^{-1}$ which is given by

$$J_{\mathbf{v}}^{-1} = \left[J^{+} + \hat{\mathbf{n}}_J \mathbf{w}^T \,\vdots\, \frac{\hat{\mathbf{n}}_J}{\hat{\mathbf{n}}_J \cdot \mathbf{v}} \right] \tag{7}$$

where once again $\hat{\mathbf{n}}_J$ is a unit length null vector of J and

$$\mathbf{w} = \frac{-(J^{+})^T \mathbf{v}}{\hat{\mathbf{n}}_J \cdot \mathbf{v}}. \tag{8}$$

Choosing an augmenting row that is a gradient results in a repeatable control strategy [12]. Thus the augmented task-space approach is one of a number of commonly used techniques for resolving manipulator redundancy [1, 4, 6, 11]. For the extended Jacobian [2], the augmenting vector is given by the gradient of $\nabla g \cdot \mathbf{n}_J$ where g is some criterion function of θ. By including this additional function the manipulator acts 'mathematically' like a nonredundant manipulator assuming that the rows of J and $\mathbf{v}$ are linearly independent. A set of these gradients can be used to define a class of control strategies which are repeatable in simply-connected, singularity-free domains [3].

One chortcoming of applying augmenting techniques is the possible introduction of artificial singularities, called algorithmic singularities [2]. These singularities are distinct from the kinematic singularities of the manipulator and are a function of the augmenting vector $\mathbf{v}$. The configurations corresponding to an algorithmic singularity are characterized by

$$\mathbf{n}_J \cdot \mathbf{v} = 0. \tag{9}$$

The presence of algorithmic singularities can seriously restrict the workspace in which the manipulator can operate as desired. A further discussion of this problem will be presented later.

This paper considers the problem of choosing an optimal control strategy from a set of repeatable strategies which have been characterized by their augmenting vectors. An example of a set of augmenting vectors which yield repeatable control strategies is the span of N linearly independent gradient functions $\{\mathbf{v}_1, \mathbf{v}_2, \ldots, \mathbf{v}_N\}$. For this case the augmenting vectors would have the form $\mathbf{v} = \sum_{i=1}^{N} a_i \mathbf{v}_i$ where each a_i is a real constant. Several considerations should be made in choosing such a basis. One should be careful to select the gradient functions to be linearly independent from the row space of the Jacobian since failure to do so will result in a singular augmented Jacobian. Secondly it should be noted that all nonzero multiples of an augmenting vector result in the same control. Thus choosing an optimal augmenting vector becomes a constrained optimization problem in which each augmenting vector is normalized. Such a normalization can be done for example by requiring that $\sum_{i=1}^{N} a_i^2 = 1$.

Now that a procedure for generating repeatable strategies has been given, it is possible to consider optimal strategies. In this work, optimality will be in terms of nearness to a desired nonrepeatable strategy. The nearest optimal repeatable control strategy (NORCS) is defined as the repeatable control strategy which is nearest to some desired nonrepeatable strategy in some region of the joint space. In general, this optimization will be performed over a set of prescribed repeatable strategies. The measure of the distance between a desired inverse G_d and a repeatable inverse G_r is defined by

$$\frac{1}{|\Omega|}\|G_r - G_d\|_\Omega^2 = \frac{1}{|\Omega|}\int_\Omega \|G_r - G_d\|_2^2 \, \mathrm{d}\theta \tag{10}$$

where $|\Omega|$ is the volume of $\Omega \subset \mathbb{R}^n$, $\|\cdot\|_2$ is the induced 2-norm for a matrix, and $\int_\Omega \mathrm{d}\theta$ is an n-dimensional integral over a simply-connected, singularity-free subset Ω of the joint space. Equation (10) provides a measure of the closeness of two inverses on some important subset Ω of the joint space. The nearest repeatable control strategy to the desired inverse G_d is defined to be the repeatable inverse G_r which minimizes (10). The subset Ω may be chosen based on some optimal configuration at which one would like the manipulator to operate. From (5) it follows that the induced 2-norm of the difference between the inverses G_r and G_d is

$$\|G_r - G_d\|_2 = \left\|\hat{\mathbf{n}}_J\left(\mathbf{w}_r^T - \mathbf{w}_d^T\right)\right\|_2 = \|\mathbf{w}_r - \mathbf{w}_d\|_2 \tag{11}$$

where the vectors $\mathbf{w}_r$ and $\mathbf{w}_d$ uniquely determine G_r and G_d, respectively. Thus the measure given in (10) for a repeatable inverse and a desired inverse becomes

$$\|G_r - G_d\|_\Omega^2 = \int_\Omega \|\mathbf{w}_r - \mathbf{w}_d\|_2 \, \mathrm{d}\theta \tag{12}$$

where $\mathbf{w}$ is given by (8).

Optimizing (12) can be rather difficult since it will, in general, be a highly nonlinear equation. Even when a minimum is obtained, it is difficult to determine whether it is in fact a global minimum. A more computationally efficient optimization can be developed by considering a slightly different problem. Rather than directly minimizing the difference of the inverses themselves, it is possible to minimize the difference of their associated null spaces. Before proceeding further, a discussion of the notion of the associated null space is in order.

An associated null vector[†] $\mathbf{n}_G$ of G is defined to be a null vector of G^T. The associated null space of G is simply the null space of G^T. The pseudoinverse has $\mathbf{n}_J$ as its associated null vector so that the null space of J and the associated null space of the pseudoinverse of J are identical. For the case of a single degree of redundancy, the associated null space is determined by the augmenting vector $\mathbf{v}$ as given in (6). In this case the associated null space is a vector-function space which, when evaluated at nonsingular configurations, is characterized by a single vector. Thus the space can be characterized by a single vector field. If this vector field is $\mathbf{n}_J$ for example, then the resulting inverse is the pseudoinverse. If the vector field is a gradient, the resulting inverse will have the desirable property of being repeatable in certain regions of the joint space. Thus certain properties of G can be identified by examining $\mathbf{n}_G$.

An additional method of quantifying the distance between two control strategies, as opposed to (10), is to define a measure between their associated null vectors. The null space approximation method (NUSAM) chooses a repeatable inverse G_r to approximate G_d by selecting the augmenting vector $\mathbf{v}$, once again from a space of gradients, which is closest to the set of associated null vectors $\mathbf{n}_{G_d}$ which have been normalized in the sense that $\int_\Omega \|\mathbf{n}_{G_d}\|_2^2 \, \mathrm{d}\theta = 1$. Thus the NUSAM criterion is

$$\min_{\substack{\mathbf{v}\in\mathcal{V}\\ \mathbf{n}\in\mathcal{N}}} \|\mathbf{v} - \mathbf{n}\|_\Omega^2 = \min_{\substack{\mathbf{v}\in\mathcal{V}\\ \mathbf{n}\in\mathcal{N}}} \int_\Omega \|\mathbf{v} - \mathbf{n}\|_2^2 \mathrm{d}\theta \tag{13}$$

[†] An associated null vector $\mathbf{n}_G$ is also commonly referred to as a left null vector of G.

where $\mathcal{V}$ is the space of allowable augmenting vectors and $\mathcal{N}$ is the set of continuous associated null vectors of G_d satisfying $\int_\Omega \|\mathbf{n}\|_2^2 \, d\theta = 1$. For the case of the pseudoinverse, the elements of $\mathcal{N}$ have the form

$$\alpha \hat{\mathbf{n}}_J \tag{14}$$

where α is in $\mathcal{A}$, the set of continuous real functions on Ω satisfying $\int_\Omega \alpha^2 \, d\theta = 1$. For the remainder of this paper, the pseudoinverse will be used as an example of a desired nonrepeatable inverse, G_d. All of the results developed apply to any other generalized inverse G_d by replacing $\mathbf{n}_J$ with $\mathbf{n}_{G_d}$.

Calculating the NUSAM solution requires several steps. The presentation that follows summarizes the key points. Additional details are available in [10]. First, note that to do actual calculations, the set of allowable augmenting vectors $\mathcal{V}$ will be taken to be the linear span of an orthonormal set $\{\mathbf{v}_1, \ldots, \mathbf{v}_N\}$ of N gradients where orthogonality will be determined by the inner product

$$\langle \mathbf{u}, \mathbf{v} \rangle_\Omega = \int_\Omega \mathbf{u} \cdot \mathbf{v} \, d\theta. \tag{15}$$

Note that it has been implicity assumed that $\mathcal{V}$ is contained in $\mathcal{L}_2(\Omega)$, the space of Lebesgue measurable n-vector functions satisfying $\int_\Omega \|\mathbf{u}\|_2^2 d\theta < \infty$.

Next, the optimization is reduced to a search over the scalar functions α. This is done by noting that for any fixed $\mathbf{n} = \alpha \hat{\mathbf{n}}_J$, the allowable augmenting vector minimizing (13) is simply the orthogonal projection of $\mathbf{n}$ onto $\mathcal{V}$

$$\mathbf{v}(\alpha) = \sum_{i=1}^{N} a_i \mathbf{v}_i \tag{16}$$

where $a_i = \langle \alpha \mathbf{n}_J, \mathbf{v}_i \rangle_\Omega$. The optimal $\mathbf{v}$ will have this form for some α and the minimization of (13) can therefore be performed over the set of possible α's. Using a Calculus of Variations argument, it can be shown [10] that an optimal α has the form

$$\alpha = \sum_{j=1}^{N} b_j \hat{\mathbf{n}}_J \cdot \mathbf{v}_j. \tag{17}$$

One then has that the Fourier coefficients of (16) are

$$a_i = \int_\Omega \alpha \hat{\mathbf{n}}_J \cdot \mathbf{v}_i \, d\theta = \sum_{j=1}^{N} M_{ij} b_j \tag{18}$$

where

$$M_{ij} = \int_\Omega (\hat{\mathbf{n}}_J \cdot \mathbf{v}_i)(\hat{\mathbf{n}}_J \cdot \mathbf{v}_j) \, d\theta. \tag{19}$$

Since each α is normalized, it follows that

$$1 = \int_\Omega \alpha^2 d\theta = \sum_{i=1}^{N} \sum_{j=1}^{N} M_{ij} b_i b_j. \tag{20}$$

In matrix-vector notation (18) and (20) become

$$\mathbf{a} = M\mathbf{b} \tag{21}$$

$$\mathbf{b}^T M \mathbf{b} = 1 \tag{22}$$

where $\mathbf{a} = [a_1 a_2 \cdots a_N]^T$, $\mathbf{b} = [b_1 b_2 \cdots b_N]^T$, and the Gramian matrix M is $M = [M_{ij}]$.

By noting that $\|\alpha \hat{\mathbf{n}}_J\|_\Omega = 1$,

$$\|\mathbf{v}(\alpha)\|_\Omega^2 = \sum_{i=1}^{N} a_i^2 = \mathbf{a}^T \mathbf{a}, \tag{23}$$

and that $\mathbf{v}(\alpha)$ is the orthogonal projection of $\alpha \mathbf{n}_J$ onto $\mathcal{V}$, one has that the α which minimizes (13) satisfies

$$\begin{aligned} \|\alpha \hat{\mathbf{n}}_J - \mathbf{v}(\alpha)\|_\Omega^2 &= \|\alpha \hat{\mathbf{n}}_J\|_\Omega^2 - \|\mathbf{v}(\alpha)\|_\Omega^2 \\ &= 1 - \mathbf{a}^T \mathbf{a}. \end{aligned} \tag{24}$$

Thus the optimization problem becomes to minimize $1 - \mathbf{a}^T \mathbf{a}$ subject to $\mathbf{b}^T M \mathbf{b} = 1$, or equivalently,

$$\begin{aligned} &\text{Maximize } \mathbf{a}^T \mathbf{a} \\ &\text{Subject to } \mathbf{b}^T M \mathbf{b} = 1. \end{aligned} \tag{25}$$

It can be shown that this is maximized when $\mathbf{a}$ and $\mathbf{b}$ are appropriately scaled singular vectors associated with the largest singular value of M (see the Appendix).

As well as providing a tool for calculating the optimal solution for a given basis the Gramian formulation also provides a measure for comparing any other augmenting vector. For an augmenting vector $\mathbf{v}$ the Gramian matrix with respect to the normalized vector function $\tilde{\mathbf{v}} = \mathbf{v}/\|\mathbf{v}\|_\Omega$ is a scalar given by

$$m'(\mathbf{v}) = \int_\Omega (\hat{\mathbf{n}}_J \cdot \tilde{\mathbf{v}})(\hat{\mathbf{n}}_J \cdot \tilde{\mathbf{v}}) \, d\theta = \frac{1}{\|\mathbf{v}\|_\Omega^2} \int_\Omega (\hat{\mathbf{n}}_J \cdot \mathbf{v})(\hat{\mathbf{n}}_J \cdot \mathbf{v}) \, d\theta. \tag{26}$$

Note that maximizing (26) over $\mathcal{V}$ is equivalent to (13). If $\mathbf{v}$ is in the span of the basis $\{\mathbf{v}_1, \ldots, \mathbf{v}_N\}$ then the Gramian matrix M can be directly used to determine

how close a match $\mathbf{v}$ is to the null space. The vector function $\mathbf{v}$ has the form $\mathbf{v} = \sum_{i=1}^{N} c_i \mathbf{v}_i$ for some set of real constant scalars $c_1, c_2, \ldots, c_N$. Representing $\mathbf{v}$ in the vector form $\mathbf{c} = [c_1 \cdots c_N]^T$ one obtains that

$$m' = \frac{\mathbf{c}^T M \mathbf{c}}{\mathbf{c}^T \mathbf{c}}. \tag{27}$$

The closer m' is to its maximum value of one, the closer $\mathbf{v}$ is to approximating a null vector of the desired inverse.

3. A Comparison of the Two Methods

This section compares the behaviour of the two methods presented above by illustrating their comparative advantages and disadvantages on a very simple manipulator. An understanding of the characteristics of these two methods will then be used to develop a combined technique, which is suitable for more general manipulators, in the following section. In all cases, the pseudoinverse will be used as a representative desired but nonrepeatable control strategy. First, consider the planar manipulator shown in Figure 1 which consists of two orthogonal prismatic joints and a third revolute joint of unit length (a PPR manipulator). This manipulator has as its Jacobian

$$J = \begin{bmatrix} 1 & 0 & -\sin\theta_3 \\ 0 & 1 & \cos\theta_3 \end{bmatrix} \tag{28}$$

and a unit length null vector $\hat{\mathbf{n}}_J = 1/\sqrt{2}[\sin\theta_3 \quad -\cos\theta_3 \quad 1]^T$. It is desired to find a repeatable inverse as a function of θ_3 which is close to the pseudoinverse

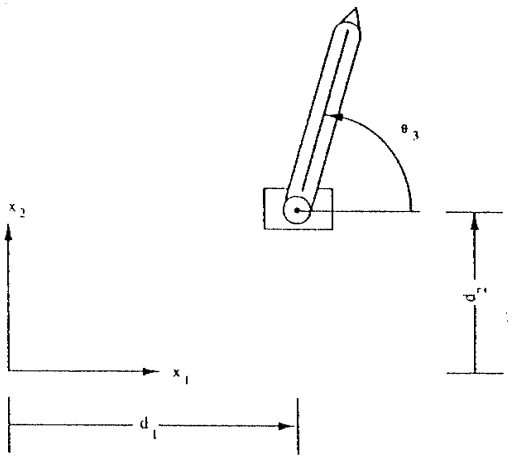

Fig. 1. Geometry of a planar three-link manipulator whose first two joints are prismatic and whose last joint is revolute and of unit link length.

in the sense of equation (10). This will be done for three different regions of interest ranging from θ_3 intervals of $[-\pi, \pi]$ to $[-\pi/4, \pi/4]$.

The manipulator in this example is simple enough to analytically calculate the nearest repeatable inverses for infinite dimensional augmenting spaces. In particular, for the set of all repeatable inverses which are functions of θ_3 only, it has been shown [9] that the nearest optimal repeatable inverse G_r is characterized by

$$\mathbf{w} = \frac{k\cos\theta_3 + \sin\theta_3}{\sqrt{2}(k^2+1)} [1 \quad -k]^T \tag{29}$$

where $\mathbf{w}$ satisfies $G_r = J^+ + \hat{\mathbf{n}}_J \mathbf{w}^T$. This solution is parameterized by the scalar k which is determined by the limits of integration. For θ_3 regions of interest that are symmetric around $\theta_3 = 0$ and smaller than $[-\pi/2, \pi/2]$, k is identically zero so that the optimal augmenting row is given by

$$\mathbf{v}^T = [0 \quad -\cos\theta_3 \quad 1 + \sin^2\theta_3]. \tag{30}$$

Symmetric regions of interest that are between the ranges of $[-\pi/2, \pi/2]$ and $[-\pi, \pi]$ are optimized by $k = \infty$ which results in

$$\mathbf{v}^T = [\sin\theta_3 \quad 0 \quad 1 + \cos^2\theta_3]. \tag{31}$$

The repeatable strategies resulting from (30) and (31) match the pseudoinverse at θ_3 values of 0 and $\pm\pi/2$, respectively. Also, note that the resulting inverse is very well behaved since the norm of the vector $\mathbf{w}$ is bounded by $1/\sqrt{2}$, so that there are no algorithmic singularities. The properties of these optimal inverses are discussed in greater detail in [9].

In general, it is not possible to analytically calculate the nearest repeatable control strategy. However, as discussed above, one can consider control strategies which are obtained by augmenting the Jacobian with a gradient row that is calculated from some finite basis of gradient vectors. For this example it is sufficient to consider augmenting rows which are gradients and functions of θ_3 only. To illustrate the effects of using different sets of allowable augmenting vectors the following bases will be considered

$$\begin{aligned}
\mathcal{B}_3 &= \{\mathbf{e}_1, \mathbf{e}_2, \mathbf{e}_3\} \\
\mathcal{B}_5 &= \mathcal{B}_3 \cup \{\cos\theta_3\mathbf{e}_3, \ \sin\theta_3\mathbf{e}_3\} \\
\mathcal{B}_5' &= \mathcal{B}_3 \cup \{\cos 2\theta_3\mathbf{e}_3, \sin 2\theta_3\mathbf{e}_3\} \\
\mathcal{B}_5'' &= \mathcal{B}_3 \cup \{\cos 4\theta_3\mathbf{e}_3, \sin 4\theta_3\mathbf{e}_3\} \\
\mathcal{B}_7 &= \mathcal{B}_5 \cup \{\cos 2\theta_3\mathbf{e}_3, \sin 2\theta_3\mathbf{e}_3\} \\
\mathcal{B}_7' &= \mathcal{B}_5' \cup \{\cos 4\theta_3\mathbf{e}_3, \sin 4\theta_3\mathbf{e}_3\} \\
\mathcal{B}_7'' &= \mathcal{B}_5'' \cup \{\cos 8\theta_3\mathbf{e}_3, \sin 8\theta_3\mathbf{e}_3\}
\end{aligned} \tag{32}$$

where $\mathbf{e}_1$, $\mathbf{e}_2$ and $\mathbf{e}_3$ are the standard basis elements for $\mathbb{R}^3$. The simplest of these bases is $\mathcal{B}_3$ which corresponds to constant terms for each element of the augmenting vector, or the 'DC' components. The next set of bases, i.e. $\mathcal{B}_5$, $\mathcal{B}_5'$ and $\mathcal{B}_5''$, correspond to the addition of the fundamental frequency for the three different Ω regions under consideration, i.e. $[-\pi, \pi]$, $[-\pi/2, \pi/2]$ and $[-\pi/4, \pi/4]$. Likewise the bases $\mathcal{B}_7$, $\mathcal{B}_7'$ and $\mathcal{B}_7''$ include an additional harmonic to the DC terms and the fundamental frequency for the three regions under consideration.

Before considering the performance of the two methods using the proposed finite bases presented, it is instructive to consider how much information is being lost by going from an infinite dimensional basis to one of such relatively small dimension. This can be done by calculating the Fourier series representation for the analytically optimal augmenting vector given by (29). As an example, consider the region $[-\pi/4, \pi/4]$ for which (30) gives an optimal augmenting vector. Since all scalar multiples result in the same control one can divide by $-\cos\theta_3$ to obtain the optimal augmenting vector

$$\mathbf{v}^T = \begin{bmatrix} 0 & 1 & \dfrac{1+\sin^2\theta_3}{-\cos\theta_3} \end{bmatrix} \tag{33}$$

which is in the space spanned by $\mathcal{B}_\infty''$. The first three terms of the Fourier series expansion for the third element of this augmenting vector are given by

$$\frac{1+\sin^2\theta_3}{-\cos\theta_3} \approx -1.3341 + 0.3061\sqrt{2}\cos 4\theta_3 - 0.0900\sqrt{2}\cos 8\theta_3 \tag{34}$$

which would correspond to its approximate representation in the basis $\mathcal{B}_7''$. Clearly, the coefficients for the basis functions are rapidly decreasing for higher harmonics indicating that the vast majority of the energy is contained in the lower frequencies. This statement can be quantified by integrating over the entire region of interest to obtain

$$\begin{aligned} \frac{2}{\pi}\int_{-\pi/4}^{\pi/4}\left[\frac{1+\sin^2(\theta_3)}{-\cos(\theta_3)}\right]^2 d\theta_3 &= 1.9113 \\ &\approx 1.3341^2 + 0.3061^2 + 0.0900^2 \\ &= 1.7798 + 0.0937 + 0.0081 \\ &= 1.8816. \end{aligned} \tag{35}$$

These numbers indicate that one would expect the optimal inverses calculated using the two methods described to be able to reasonably approximate the analytically optimal inverse even when using a small number of basis functions.

To determine the actual nearest optimal repeatable control strategy (NORCS) for the finite bases of (32), one must evaluate the integral given in (12), where the integrand in this case is simply given by (8) since J^+ is the desired inverse, over the $N-1$ dimensional space of normalized coefficients for the basis functions. The results of performing this optimization for the various different integration intervals and augmenting bases is summarized in Table I. The data in Table I validates, for the most part, the hypothesis concerning the ability of a small number of basis functions to approximate the analytically optimal solution. In fact, using only the DC terms, i.e., those represented by the basis $\mathcal{B}_3$, provides a very reasonable approximation of the analytical optimal for both of the smaller Ω intervals. Even in the largest Ω interval the DC terms tend to dominate the higher harmonics. The fact that the NORCS solutions in the largest interval do not represent a particularly good approximation to the analytically optimal solution is due to its different form in this region which results in a singularity in its representation as a gradient, i.e. dividing through by $\sin\theta_3$ results in a singularity at $\theta_3 = 0$, the center of the Ω integration interval. Unlike the case where $\Omega = [-\pi/4, \pi/4]$ the infinite augmenting basis that would result from expanding $\mathcal{B}_7$ would not include the analytically optimal solution.

The additional effect of the size of the integration interval, as would be expected, is that the resulting repeatable inverses more closely resemble the desired pseudoinverse as the desired region of operation becomes smaller and smaller. This is graphically illustrated in Figs 2–4. Note, however, that while reducing

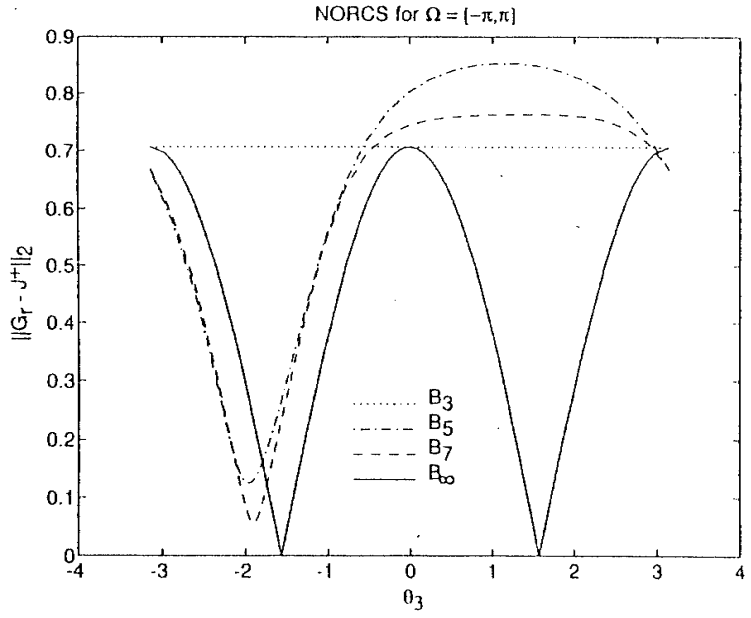

Fig. 2. A plot of $\|G_r - J^+\|_2$ for the four nearest optimal repeatable control strategies as a function of θ_3 for the PPR manipulator shown in Fig. 1. This quantity represents the cost of requiring the control strategy to be repeatable. Each optimal strategy was calculated for a θ_3 region of $[-\pi, \pi]$.

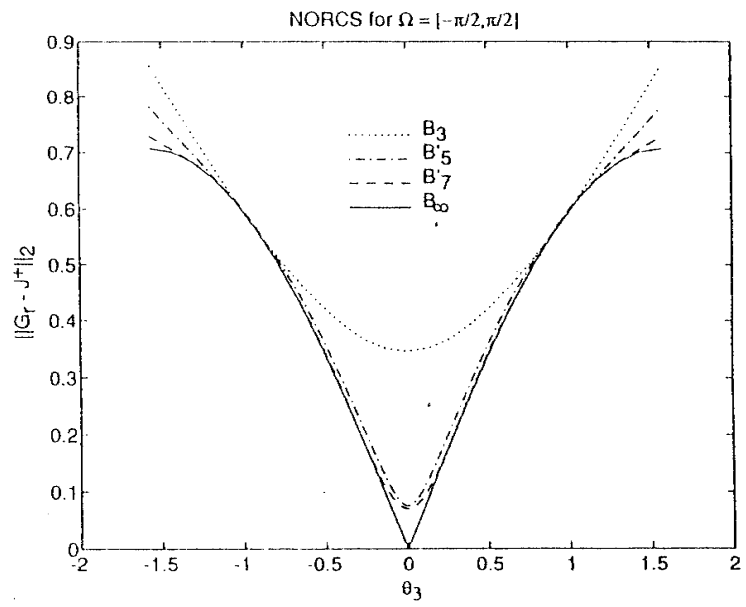

Fig. 3. A plot of $\|G_r - J^+\|_2$ for the four nearest optimal repeatable control strategies as a function of θ_3 for the PPR manipulator shown in Fig. 1. This time each optimal strategy was calculated for a θ_3 region of $[-\pi/2, \pi/2]$.

the Ω integration interval results in better performance within that interval it also tends to correspond with markedly poorer performance just outside of the interval as is clearly evident in Fig. 5. Thus even though higher-dimensional augmenting bases do not dramatically improve the performance of the resulting inverse within the specified region Ω (particularly if this region is small), it still may be useful to retain some of the higher harmonics in order to maintain reasonable behaviour outside of the region Ω. Finally, it is important to note that inverses with similar figures of merit may provide radically different performance over the desired region of operation.

As the Ω integration interval becomes smaller and smaller, its limiting value is a single point in the joint space at which the optimal augmenting row clearly becomes the transpose of the null vector of the Jacobian $\mathbf{n}_J$ evaluated at that particular value of θ. This can be clearly seen in Table I for the smallest Ω integration interval where the augmenting row is approaching $\hat{\mathbf{n}}_J^T(0) = [0 \ -0.7071 \ 0.7071]$. This is one of the fundamental observations about which the null space approximation method (NUSAM) is based. This technique attempts to retain the characteristics of the NORCS inverse by performing the much simpler optimization represented by (13). The results of applying this optimization using the same augmenting bases and Ω intervals as in the NORCS case are summarized in Table II. Note that since the goal of this optimization is the approximation of the

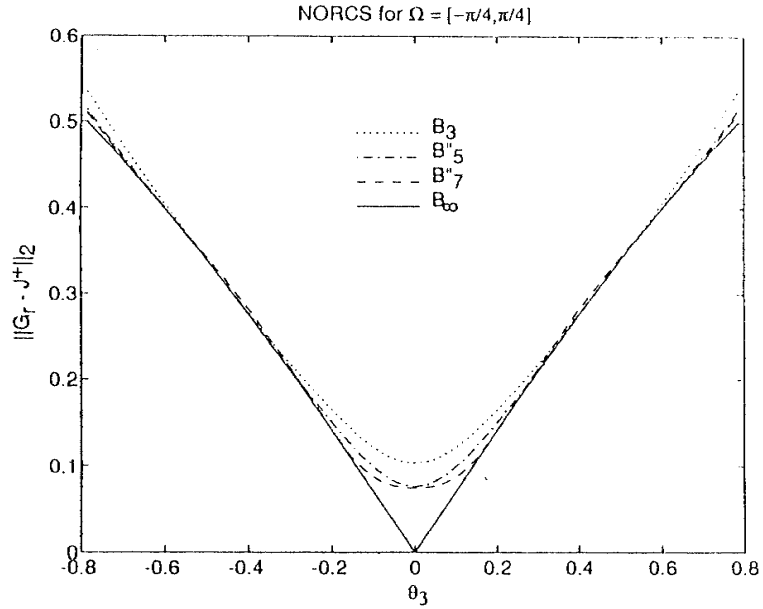

Fig. 4. A plot of $\|G_r - J^+\|_2$ for the four nearest optimal repeatable control strategies as a function of θ_3 for the PPR manipulator shown in Fig. 1. This time each optimal strategy was calculated for a θ_3 region of $[-\pi/4, \pi/4]$.

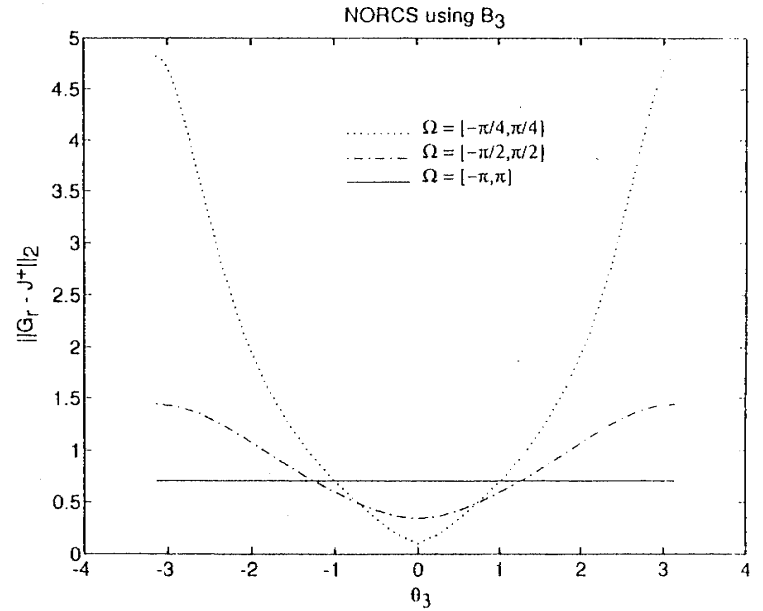

Fig. 5. A plot of $\|G_r - J^+\|_2$ for the nearest optimal repeatable control strategies using a basis of B_3 for the θ_3 regions of $[-\pi, \pi]$, $[-\pi/2, \pi, 2]$ and $[-\pi/4, \pi/4]$.

Table I. Optimal augmentig rows using the nearest optimal repeatable control strategy (NORCS)

$\Omega \equiv \theta_3 \in [-\pi, \pi]$

Basis	$(1/\lvert\Omega\rvert)\lVert G_r - J^+\rVert_\Omega^2$	Optimal augmenting row
$\mathcal{B}_3$	0.5000	$[0.0000 \quad 0.0000 \quad 1.000]$
$\mathcal{B}_5$	0.4690	$[0.1392 \quad -0.0507 \quad -0.8399 - 0.1504\sqrt{2}\cos\theta_3 - 0.5000\sqrt{2}\sin\theta_3]$
$\mathcal{B}_7$	0.4111	$[0.0649 \quad -0.0222 \quad -0.7846 - 0.2110\sqrt{2}\cos\theta_3 - 0.5709\sqrt{2}\sin\theta_3 + 0.0677\sqrt{2}\cos 2\theta_3 - 0.0678\sqrt{2}\sin 2\theta_3]$
$\mathcal{B}_\infty$	0.2500	$[\sin\theta_3 \quad 0.0000 \quad 1.0000 + \cos^2\theta_3]$

$\Omega \equiv \theta_3 \in [-\pi/2, \pi/2]$

Basis	$(1/\lvert\Omega\rvert)\lVert G_r - J^+\rVert_\Omega^2$	Optimal augmenting row
$\mathcal{B}_3$	0.3170	$[0.0000 \quad -0.3238 \quad 0.9461]$
$\mathcal{B}_5'$	0.2665	$[0.0000 \quad -0.3214 \quad 0.8830 - 0.3420\sqrt{2}\cos 2\theta_3]$
$\mathcal{B}_7'$	0.2540	$[0.0000 \quad -0.2283 \quad 0.7905 - 0.5412\sqrt{2}\cos 2\theta_3 + 0.1796\sqrt{2}\cos 4\theta_3]$
$\mathcal{B}_\infty$	0.2500	$[0.0000 \quad -\cos\theta_3 \quad 1.0000 + \sin^2\theta_3]$

$\Omega \equiv \theta_3 \in [-\pi/4, \pi/4]$

Basis	$(1/\lvert\Omega\rvert)\lVert G_r - J^+\rVert_\Omega^2$	Optimal augmenting row
$\mathcal{B}_3$	0.0985	$[0.0000 \quad -0.5971 \quad 0.8021]$
$\mathcal{B}_5''$	0.0936	$[0.0000 \quad -0.6330 \quad 0.7544 - 0.1736\sqrt{2}\cos 4\theta_3]$
$\mathcal{B}_7''$	0.0932	$[0.0000 \quad -0.5874 \quad 0.7890 - 0.1734\sqrt{2}\cos 4\theta_3 - 0.0485\sqrt{2}\cos 8\theta_3]$
$\mathcal{B}_\infty$	0.0908	$[0.0000 \quad -\cos\theta_3 \quad 1.0000 + \sin^2\theta_3]$

Augmenting bases
$\mathcal{B}_3 = \{k_1\mathbf{e}_1, k_1\mathbf{e}_2, k_1\mathbf{e}_3\}$
$\mathcal{B}_5 = \mathcal{B}_3 \cup \{k_2\cos\theta_3\mathbf{e}_3, k_2\sin\theta_3\mathbf{e}_3\}$ $\mathcal{B}_5' = \mathcal{B}_3 \cup \{k_2\cos 2\theta_3\mathbf{e}_3, k_2\sin 2\theta_3\mathbf{e}_3\}$ $\mathcal{B}_5'' = \mathcal{B}_3 \cup \{k_2\cos 4\theta_3\mathbf{e}_3, k_2\sin 4\theta_3\mathbf{e}_3\}$
$\mathcal{B}_7 = \mathcal{B}_5 \cup \{k_2\cos 2\theta_3\mathbf{e}_3, k_2\sin 2\theta_3\mathbf{e}_3\}$ $\mathcal{B}_7' = \mathcal{B}_5' \cup \{k_2\cos 4\theta_3\mathbf{e}_3, k_2\sin 4\theta_3\mathbf{e}_3\}$ $\mathcal{B}_7'' = \mathcal{B}_5'' \cup \{k_2\cos 8\theta_3\mathbf{e}_3, k_2\sin 8\theta_3\mathbf{e}_3\}$
$k_1 = 1/\sqrt{\lvert\Omega\rvert}$ and $k_2 = \sqrt{2/\lvert\Omega\rvert}$

desired null vector, the accuracy of this approximation is quantified by m', which in this case is the maximum singular value of M, i.e., $\sigma_1(M)$. Table III provides a direct comparison between the two techniques by comparing both figures of merit, i.e. the error in approximating the desired inverse, $1/|\Omega|\,\|G_r - J^+\|_\Omega^2$, which is the true minimization criteria, as well as the error in approximating the null vector of the desired inverse, $\min \|\mathbf{v} - \mathbf{n}_J\|_\Omega^2 = 1 - m'(\mathbf{v})$.

Table II. Optimal augmentig rows using the null-space approximation method (NUSAM)

$\Omega \equiv \theta_3 \in [-\pi, \pi]$

Basis	$m' = \sigma_1(M)$	Optimal augmenting row
$\mathcal{B}_3$	0.5000	$[0.0000 \quad 0.0000 \quad 1.0000]$
$\mathcal{B}_5$	0.7500	$[0.5774 \quad 0.0000 \quad 0.8165\sqrt{2}\sin\theta_3]$
$\mathcal{B}_7$	0.7500	$[0.5774 \quad 0.0000 \quad 0.8165\sqrt{2}\sin\theta_3$
–	0.3750	$[0.0000 \quad -0.7071 \quad 0.7071] = \hat{\mathbf{n}}_J^T(0)$

$\Omega \equiv \theta_3 \in [-\pi/2, \pi/2]$

Basis	$m' = \sigma_1(M)$	Optimal augmenting row
$\mathcal{B}_3$	0.7170	$[0.0000 \quad -0.5632 \quad 0.8263]$
$\mathcal{B}_5'$	0.7484	$[0.0000 \quad -0.5767 \quad 0.7389 + 0.3483\sqrt{2}\cos 2\theta_3]$
$\mathcal{B}_7'$	0.7496	$[0.0000 \quad -0.5772 \quad 0.7360 + 0.3469\sqrt{2}\cos 2\theta_3 - 0.0693\sqrt{2}\cos 4\theta_3]$
–	0.6933	$[0.0000 \quad -0.7071 \quad 0.7071] = \hat{\mathbf{n}}_J^T(0)$

$\Omega \equiv \theta_3 \in [-\pi/4, \pi/4]$

Basis	$m' = \sigma_1(M)$	Optimal augmenting row
$\mathcal{B}_3$	0.9070	$[0.0000 \quad -0.6707 \quad 0.7418]$
$\mathcal{B}_5''$	0.9090	$[0.0000 \quad -0.6708 \quad 0.7383 + 0.0696\sqrt{2}\cos 4\theta_3]$
$\mathcal{B}_7''$	0.9091	$[0.0000 \quad -0.6708 \quad 0.7381 + 0.0696\sqrt{2}\cos 4\theta_3 - 0.0166\sqrt{2}\cos 8\theta_3]$
–	0.9048	$[0.0000 \quad -0.7071 \quad 0.7071] = \hat{\mathbf{n}}_J^T(0)$

Augmenting bases
$\mathcal{B}_3 = \{k_1\mathbf{e}_1, k_1\mathbf{e}_2, k_1\mathbf{e}_3\}$
$\mathcal{B}_5 = \mathcal{B}_3 \cup \{k_2\cos\theta_3\mathbf{e}_3, k_2\sin\theta_3\mathbf{e}_3\}$ $\mathcal{B}_5' = \mathcal{B}_3 \cup \{k_2\cos 2\theta_3\mathbf{e}_3, k_2\sin 2\theta_3\mathbf{e}_3\}$ $\mathcal{B}_5'' = \mathcal{B}_3 \cup \{k_2\cos 4\theta_3\mathbf{e}_3, k_2\sin 4\theta_3\mathbf{e}_3\}$
$\mathcal{B}_7 = \mathcal{B}_5 \cup \{k_2\cos 2\theta_3\mathbf{e}_3, k_2\sin 2\theta_3\mathbf{e}_3\}$ $\mathcal{B}_7' = \mathcal{B}_5' \cup \{k_2\cos 4\theta_3\mathbf{e}_3, k_2\sin 4\theta_3\mathbf{e}_3\}$ $\mathcal{B}_7'' = \mathcal{B}_5'' \cup \{k_2\cos 8\theta_3\mathbf{e}_3, k_2\sin 8\theta_3\mathbf{e}_3\}$
$k_1 = 1/\sqrt{\lvert\Omega\rvert}$ and $k_2 = \sqrt{2/\lvert\Omega\rvert}$

When analyzing the results of the NUSAM optimization, the general effects due to varying the augmenting bases and the Ω intervals are quite similar to those observed in the NORCS results. Overall, the DC terms tend to dominate and more accurate approximations of the null vector are obtained with smaller Ω intervals. However, it is important to point out that more accurately approximating the null vector does not correspond to more accurately approximating the perfor

Table III. A comparison of the two techniques

$\Omega \equiv \theta_3 \in [-\pi, \pi]$

	$(1/\|\Omega\|)\|G_r - J^+\|_\Omega^2$		$\min \|\mathbf{v} - \mathbf{n}_J\|_\Omega^2 = 1 - m'(\mathbf{v})$	
Basis	NORCS	NUSAM	NORCS	NUSAM
$\mathcal{B}_3$	0.5000	0.5000	0.5000	0.5000
$\mathcal{B}_5$	0.4690	*	0.5601	0.2500
$\mathcal{B}_7$	0.4111	*	0.5307	0.2500

$\Omega \equiv \theta_3 \in [-\pi/2, \pi/2]$

	$(1/\|\Omega\|)\|G_r - J^+\|_\Omega^2$		$\min \|\mathbf{v} - \mathbf{n}_J\|_\Omega^2 = 1 - m'(\mathbf{v})$	
Basis	NORCS	NUSAM	NORCS	NUSAM
$\mathcal{B}_3$	0.3170	0.4146	0.3312	0.2830
$\mathcal{B}'_5$	0.2665	1.4786	0.3782	0.2516
$\mathcal{B}'_7$	0.2540	2.5474	0.4378	0.2504

$\Omega \equiv \theta_3 \in [-\pi/4, \pi/4]$

	$(1/\|\Omega\|)\|G_r - J^+\|_\Omega^2$		$\min \|\mathbf{v} - \mathbf{n}_J\|_\Omega^2 = 1 - m'(\mathbf{v})$	
Basis	NORCS	NUSAM	NORCS	NUSAM
$\mathcal{B}_3$	0.0985	0.1045	0.1011	0.0930
$\mathcal{B}''_5$	0.0936	0.1142	0.1157	0.0910
$\mathcal{B}''_7$	0.0932	0.1153	0.1221	0.0909

* Denotes an algorithmic singularity.

mance of the desired inverse. In particular, consider the data for the case where the Ω region is $[-\pi/2, \pi/2]$ in Table III. Note that despite the fact that a larger basis (from $\mathcal{B}_3$ to $\mathcal{B}'_7$) in the optimization decreases the error in the approximation of the null vector (from 0.2830 to 0.2504) the error in approximating the desired inverse actually increases dramatically (from 0.4146 to 2.5474). Similar, though less dramatic, behaviour is apparent in the Ω interval from $[-\pi/4, \pi/4]$ and in the worst case, when Ω is from $[-\pi, \pi]$, the larger basis actually results in an augmenting vector with an algorithmic singularity within the desired operating region. From this data it would at first appear that there is no point in applying the NUSAM optimization for larger bases. In fact, one might argue that since only the DC terms are significant, why not forgo the NUSAM optimization and simply use the actual null vector evaluated at the middle of the desired interval? Indeed the vectors obtained when applying the NUSAM optimization do lie close to this value of $\hat{\mathbf{n}}_J^T(0) = [0 \quad -0.7071 \quad 0.7071]$ as expected. However, it is important to remember that similar augmenting vectors do not necessarily represent similar inverses. In particular, the matched null vector $\hat{\mathbf{n}}_J^T(0)$ results in an algorithmic singularity when $\cos\theta_3 = -1$ while none of the augmenting

vectors obtained using the NUSAM optimization with a basis of $\mathcal{B}_3$ possess any algorithmic singularities. This singularity, even if it is not located in the desired region Ω, results in significantly poorer performance, e.g. a value of 0.6221 for $1/|\Omega| \, \|G_r - J^+\|_\Omega^2$ in the region $[-\pi/2, \pi/2]$.

It may at first appear anomalous that the NUSAM optimization will result in augmenting vectors that remove potential algorithmic singularities, as in the case of the basis $\mathcal{B}_3$ for the region $[-\pi, \pi]$, while at the same time it introduces algorithmic singularities when the basis is expanded to either $\mathcal{B}_5$ or $\mathcal{B}_7$. This apparent anomaly can be resolved by examining how the NUSAM optimization treats algorithmic singularities. Clearly, vectors which produce algorithmic singularities within the desired region Ω are discouraged due to the fact that the integrand in (26) becomes zero thus explaining why the augmenting vector obtained when using $\mathcal{B}_3$ is able to eliminate the singularity that occurs when simply using $\hat{\mathbf{n}}_J^T(0)$. However, if the integrand is relatively large over most of the Ω region, it may be able to overcome the fact that it is zero at a single point. This accounts for the fact that the optimal solutions for the bases $\mathcal{B}_5$ and $\mathcal{B}_7$ contain algorithmic singularities. Note that this treatment of algorithmic singularities represents a fundamental difference between the NUSAM optimization and the NORCS method. In particular, a NORCS augmenting vector may not result in an algorithmic singularity within Ω since this causes the integrand in (2) to go to infinity. This is also more effective in preventing algorithmic singularities from

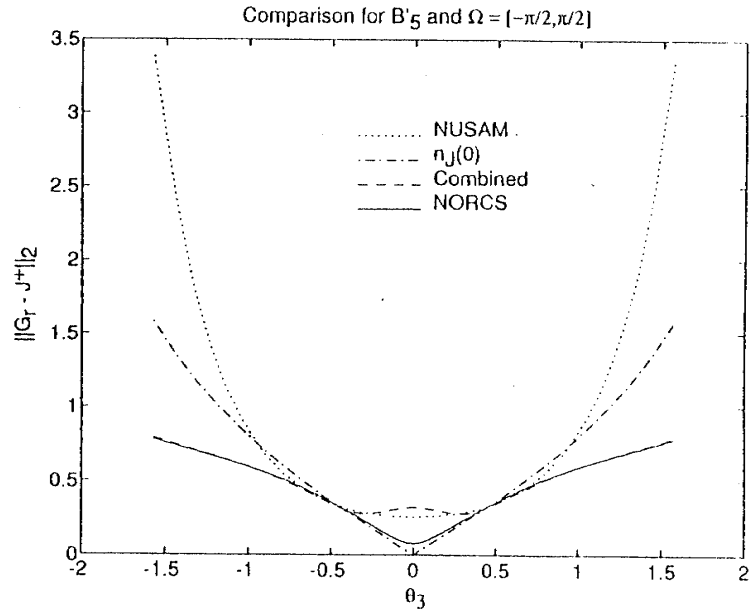

Fig. 6. A plot of $\|G_r - J^+\|_2$ for the nearest optimal repeatable method, the null-space approximation method, the combined technique, and the matched null vector for a θ_3 region $[-\pi/2, \pi/2]$ and an augmenting basis $\mathcal{B}'_5$.

even approaching the region Ω, as is clearly illustrated in Fig. 6 by comparing the values of $(1/|\Omega|)\|G_r - J^+\|_\Omega^2$ for the NUSAM and NORCS solutions.

While the inverses obtained using the NORCS technique are inherently superior in performance to those obtained through the NUSAM optimization, the NUSAM optimization has an unquestionable advantage in terms of computational efficiency. The algorithms for computing the optimal augmenting vectors both require repeated n-dimensional integrations. In the NORCS case (see (8)), the integrand requires a matrix vector product of the desired inverse with the augmenting vector, a dot product with the basis vector (a function of N) and the null vector, and a scalar division (which prevents the selection of augmenting vectors that result in algorithmic singularities). In the NUSAM case (see (19)), the integrand only requires two n-dimensional dot products using the basis vector (a function of N) and the null vector as well as a scalar multiplication. While the simpler integrand for the NUSAM case results is some computational advantage, the overwhelming savings in computation comes from the number of times this integration must be performed. In the NUSAM case, this n-dimensional integration must be performed exactly $N(N+1)/2$ times, once for every unique element of M (which is then followed by a singular value decomposition of M). In the NORCS case, the number of n-dimensional integrations is essentially unknown. In the simplest case one could form a grid in the $(N-1)$-dimensional space of normalized coefficient vectors which would result in an exponential number of n-dimensional integrations. Thus the NORCS approach quickly becomes intractable. For example, for $N = 3$ the NORCS algorithm required an order of magnitude more computation time as opposed to the NUSAM algorithm whereas for $N = 7$ NORCS required four orders of magnitude more computation time.

4. Combining NORCS and NUSAM

From the preceding section it is clear that neither NORCS or NUSAM are completely satisfactory by themselves for calculating augmenting vectors for systems with large numbers of degrees of freedom. While the nearest optimal repeatable criterion represents a better measure of closeness to the desired inverse, it rapidly becomes computationally intractable, whereas the null-space approximation method results in poorer performance primarily due to its treatment of algorithmic singularities. It is, however, possible to combine the two methods by using information from the null-space approximation method for determining optimal subspaces in which to perform a lower-dimensional search for the nearest optimal repeatable inverse. This information is contained in the complete SVD of M as opposed to simply the singular vector associated with the largest singular value. In particular, the SVD of M may be written as

$$M = \sum_{i=1}^{N} \sigma_i \hat{\mathbf{u}}_i \hat{\mathbf{u}}_i^T \tag{36}$$

where the singular values are ordered from largest to smallest. Since there is a gross correlation between matching the associated null space of the desired inverse and matching the inverse itself, the NORCS solution should be near the space spanned by the $\hat{\mathbf{u}}_i$ associated with the large singular values, and not necessarily strictly along $\hat{\mathbf{u}}_1$ as shown from the data in the previous section. Exactly what constitutes 'large' singular values is somewhat arbitrary, however the singular values range from 0 to 1 and are typically clustered so that there will be one or more values of i for which $\sigma_i \gg \sigma_{i+1}$. If this is not the case and all of the σ_i are approximately equal then there is no information that can be exploited to guide the NORCS optimization.

To illustrate the procedure for combining these techniques and to evaluate its efficacy, consider the simple example in the previous section for the case when the Ω region is given by $[-\pi/2, \pi/2]$. Assume that one would like information from the NUSAM optimization using the basis $\mathcal{B}_5'$ to perform a lower-dimensional NORCS optimization. From Table II one can see that $\sigma_1 = 0.7484$ and that $\hat{\mathbf{u}}_1 = [0.000 \;\; 0.5767 \;\; -0.7389 \;\; -0.3483 \;\; 0.000]^T$, however, the complete SVD of M is given by

$$S = \text{diag}(0.7484 \;\; 0.7001 \;\; 0.5000 \;\; 0.0499 \;\; 0.0016) \tag{37}$$

and

$$U = \begin{bmatrix} 0.0000 & -0.5548 & 0.0000 & -0.8320 & 0.0000 \\ 0.5767 & -0.0000 & -0.0000 & -0.0000 & 0.8169 \\ -0.7389 & 0.0000 & -0.4264 & -0.0000 & 0.5217 \\ -0.3483 & 0.0000 & 0.9045 & -0.0000 & 0.2459 \\ 0.0000 & -0.8320 & 0.0000 & 0.5548 & 0.0000 \end{bmatrix}. \tag{38}$$

From these singular values it is clear that many other augmenting rows would have been nearly as good an approximation to the desired null vector since the first three singular values are on the same order of magnitude. Thus an augmenting vector in the space spanned by $\hat{\mathbf{u}}_1$ $\hat{\mathbf{u}}_2$ and $\hat{\mathbf{u}}_3$ can be reasonably considered as a candidate for resulting in a nearest optimal repeatable control strategy. One can therefore run the NORCS algorithm evaluating only coefficients which are normalized linear combinations of $\hat{\mathbf{u}}_1$ $\hat{\mathbf{u}}_2$ and $\hat{\mathbf{u}}_3$, thus only requiring a two-dimensional optimization. This optimization results in the coefficients $0.6428\hat{\mathbf{u}}_1 + 0.0000\hat{\mathbf{u}}_2 + 0.7660\hat{\mathbf{u}}_3$ which corresponds to the augmenting row

$$\mathbf{v}^T = [0.0000 \quad 0.3707 \quad -0.8016 + 0.4690\sqrt{2}\cos 2\theta_3]. \tag{39}$$

The measure of difference between the inverse that corresponds to this augmenting row and the desired inverse is given by $1/|\Omega|\,\|G_r - J^+\|_\Omega^2 = 0.2978$ which is markedly better than that obtained using a two-dimensional NORCS optimization with the basis $\mathcal{B}_3$ $(1/|\Omega|\,\|G_r - J^+\|_\Omega^2 = 0.3170)$ which required

approximately the same amount of computation time. This markedly improved performance is graphically illustrated in Fig. 6. Note that the four-dimensional NORCS optimization using the basis $\mathcal{B}_5'$ resulted in $1/|\Omega|\,\|G_r - J^+\|_\Omega^2 = 0.2665$ which is the true optimal in the space spanned by $\mathcal{B}_5'$ but which required an order of magnitude more computation time. One can identify the component of this vector that lies outside of the lower-dimensional search space by multiplying by U to obtain

$$\mathbf{a}^T(\mathcal{B}_5')U = [0.7187 \quad 0 \quad 0.6859 \quad 0 \quad -0.1140] \tag{40}$$

which shows that there exists a small component strictly along $\hat{\mathbf{u}}_5$.

As a final more realistic example of applying the combination of these techniques, consider the typical 7-DOF anthropomorphic manipulator described in detail in [8]. The Jacobian for this particular manipulator is given by

$$J = \begin{bmatrix} S_2C_3C_4 + C_2S_4 & -S_3C_4 & S_4 & 0 & 0 & S_5 & -C_5S_6 \\ -S_2S_3 & -C_3 & 0 & -1 & 0 & -C_5 & -S_5S_6 \\ -S_2C_3S_4 + C_2C_4 & S_3S_4 & C_4 & 0 & 1 & 0 & C_6 \\ -S_2S_3C_4g - S_2S_3h & -C_3C_4g - C_3h & 0 & -h & 0 & 0 & 0 \\ -S_2C_3g - S_2C_3C_4h - C_2S_4h & S_3g + S_3C_4h & -hS_4 & 0 & 0 & 0 & 0 \\ S_2S_3S_4g & C_3S_4g & 0 & 0 & 0 & 0 & 0 \end{bmatrix} \tag{41}$$

where S_i and C_i denote $\sin\theta_i$ and $\cos\theta_i$ and the parameters g and h are the nonzero lengths of the upper and lower arms, respectively. The null vector for this manipulator can also be written analytically and is given by

$$\mathbf{n}_J = \begin{bmatrix} C_3S_4S_6h \\ -S_2S_3S_4S_6h \\ -(S_2g + S_2C_4h + C_2C_3S_4h)S_6 \\ 0 \\ S_2C_4S_6g + S_2S_4C_5C_6g + S_2S_6h \\ S_2S_4S_5S_6g \\ -S_2S_4C_5g \end{bmatrix}. \tag{42}$$

The link lengths g and h will be taken to be 1 meter. It is important to point out that while such an analytic expression for the null vector is desirable, it is not required. One can always numerically determine the null vector for a given configuration.

For the purposes of illustration the region of interest Ω will consist of $\theta_i \in [\pi/4, 3\pi/4]$ except for θ_5 which is in the range $[-\pi/4, \pi/4]$. The set of augmenting basis functions will consist of only the DC terms, i.e. $\mathcal{B}_7 = \{\mathbf{e}_1, \mathbf{e}_2, \mathbf{e}_3, \mathbf{e}_4, \mathbf{e}_5, \mathbf{e}_6, \mathbf{e}_7\}$. As a point of reference, the null vector (42) evaluated at the center of Ω is given by

$$\hat{\mathbf{n}}_J^T = [0.0 \quad -0.5 \quad -0.5 \quad 0.0 \quad 0.5 \quad 0.0 \quad -0.5] \tag{43}$$

and results in an inverse that has an algorithmic singularity within Ω. Performing the NUSAM optimization results in a matrix M that has the following singular values

$$S = \text{diag}(0.8154,\ 0.0653,\ 0.0515,\ 0.0417,\ 0.0232,\ 0.0029,\ 0.0000) \tag{44}$$

where $\hat{\mathbf{u}}_1$ which corresponds to the optimal augmenting row is given by

$$\mathbf{v}^T = [0.0000 \quad -0.4581 \quad -0.5196 \quad 0.0000 \quad 0.5106 \quad 0.0000 \quad -0.5094]. \tag{45}$$

The acuracy to which the resulting inverse approximates the pseudoinverse is given by $1/|\Omega|\,\|G_r - J^+\|_\Omega^2 = 0.4523$ which clearly indicates that there is no algorithmic singularity despite the fact that this vector is quite close to that given by (43). Analysis of the singular values given in (44) indicates that one would not expect to identify a significantly better inverse since there is an order of magnitude separation between the first and second singular values. In fact, running the NORCS algorithm in these lower-dimensional subspaces does not significantly alter the optimal vector from that given by (45). As a final indication of the intractability of the NORCS optimization for the entire range of $\mathcal{B}_7$, despite several days of computation time the algorithm eventually terminated in a local minima that resulted in a vector with significantly poorer performance than (45).

5. Simulations

The previous two sections have concentrated on comparing various repeatable inverses with a desired nonrepeatable inverse, in this case the pseudoinverse, using the somewhat nonintuitive metric $\|G_r - G_d\|_\Omega$, i.e., the norm of the difference between the repeatable inverse and the desired inverse over the design region of the joint space, Ω. While this metric is arguably the most appropriate, it is instructive to consider the behavior of the repeatable inverses with respect to the properties of the desired inverse. This section considers the performance of the various repeatable inverses discussed previously in a simulation of the PPR manipulator following a specific desired end-effector trajectory. It must be emphasized, however, that no single trajectory can satisfactorily represent the behaviour of an inverse over the entire range of end-effector trajectories and manipulator configurations in Ω, which is the motivation for relying on the norm $\|G_r - G_d\|_\Omega$ as the primary measure of performance.

The desired end-effector trajectory selected for the simulation studies is given in Fig. 7. The PPR manipulator depicted in Fig. 1 is commanded to follow the 4-meter square trajectory labeled ABCDE. The initial configuration of the manipulator is set to the origin of joint space which corresponds to the point A in the workspace. Since all of the repeatable inverses calculated in the previous sections have used symmetric design regions centered around $\theta_3 = 0$, this pat-

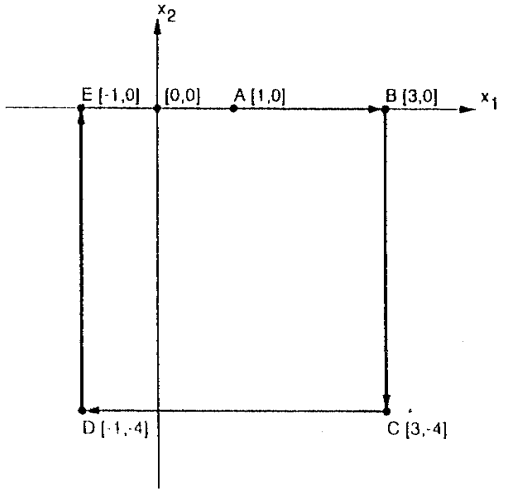

Fig. 7. The desired end-effector trajectory used in the simulation of the PPR manipulator shown in Fig. 1. The 4-meter square path starts and ends at A, which corresponds to the origin in joint space. The manipulator is commanded to traverse the trajectory in a clockwise manner with a constant speed.

the initial configuration in the center of the desired region of operation. The desired trajectory was then selected to travel away from this center region at a constant speed. The path is intentionally discontinuous in direction at the corners of the square to help distinguish points along the trajectory and to emphasize the directional nature of the inverses.

Figure 8 illustrates a view of the three-dimensional joint-space trajectory, shown in bold, that corresponds to the use of pseudoinverse control to follow the square end-effector trajectory labeled ABCDE. The other lines in this figure represent the integral surface resulting from the optimal repeatable inverse, i.e., that obtained with the basis $\mathcal{B}_\infty$. Note that the repeatable surface initially contains the pseudoinverse trajectory but that they start to diverge as the pseudoinverse trajectory leaves the design region at point C. It is at this point that the global repeatability requirement forces the repeatable inverse to abandon the desired pseudoinverse solution. The drift resulting from the pseudoinverse solution is clearly identified by the distance of the final manipulator configuration from the origin, which was the initial configuration. The spiral on which both the initial and final pseudoinverse solutions lie represents the fiber of all points corresponding to the point A in the workspace.

A quantitative comparison of the joint angle velocity required to achieve the desired end-effector trajectory is given in Fig. 9. The norm of the pseudoinverse solution and that of the optimal repeatable inverse are identical up to the point C since they follow exactly the same joint trajectory as was shown in Fig. 8. The initial divergence of these two trajectories in the region from C to D results in a

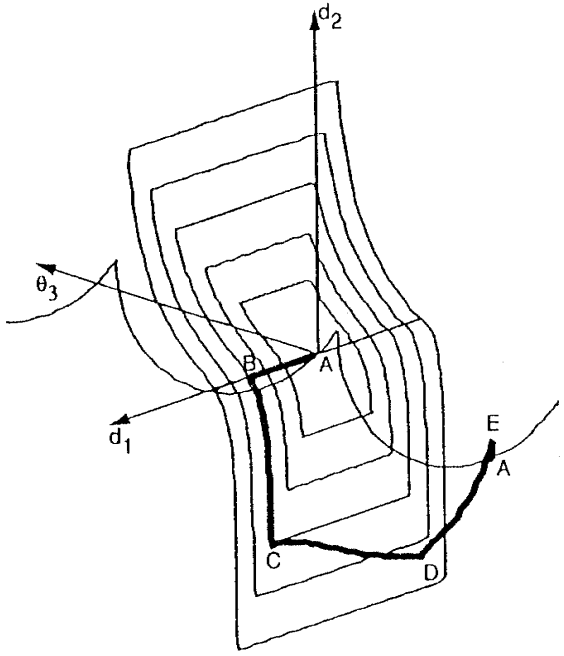

Fig. 8. A 3-D view of the joint-space trajectory resulting from using pseudoinverse control shown in bold, to follow the square end-effector trajectory given in Fig. 6, as compared to the repeatable surface obtained from the optimal repeatable control using the basis $\mathcal{B}_\infty$. Note that the repeatable surface initially contains the pseudoinverse trajectory but that they start to diverge as the pseudoinverse trajectory leaves the design region. It is at this point that the global repeatability requirement forces the repeatable inverse to abandon the desired pseudoinverse solution.

larger joint-velocity norm for the repeatable inverse due to the pseudoinverse's local optimality. However, note that immediately preceding the point E, the optimal repeatable inverse actually outperforms the pseudoinverse solution. This is not entirely unexpected since the manipulators are now at different configurations.

Three other repeatable inverses are also compared in Fig. 9. These are the NORCS inverse, the NUSAM inverse, and the combined NUSAM/NORCS inverse discussed in Section 4 for the basis $\mathcal{B}_5'$ and a design region of $\Omega = [-\pi/2, \pi/2]$. As expected, the performance of the pure NORCS technique is best, the pure NUSAM technique is the poorest, and the combined NUSAM/NORCS technique lies in between the two. First, consider the performance of the NUSAM technique. The NUSAM inverse performs well over large portions of the trajectory, however, it results in relatively large joint velocities near the points C and D. This behavior is due to the fact that, as discussed in Section 5, the NUSAM technique is susceptible to the influence of algorithmic singularities. While this particular inverse does not result in an algorithmic singularity

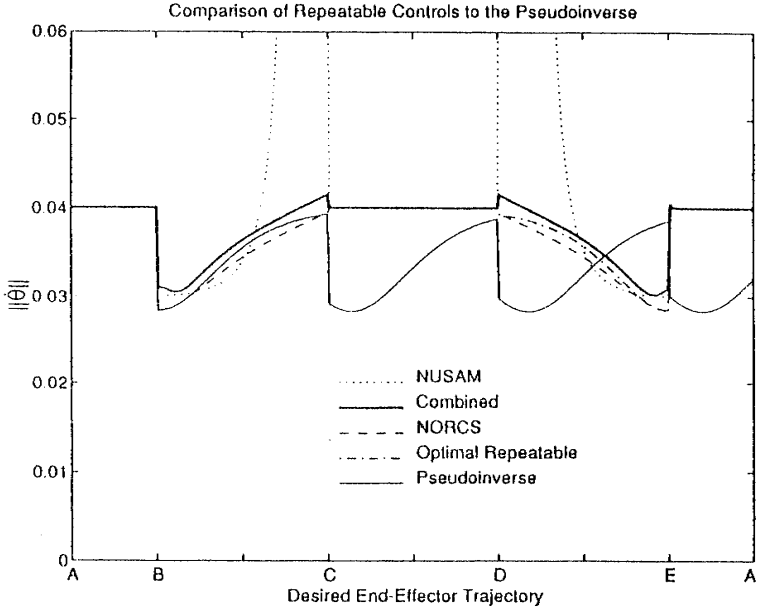

Fig. 9. A plot of the joint-velocity norm as a function of the position of the end-effector in the workspace for the trajectory shown in Fig. 7. Note that the trajectory obtained from the NUSAM inverse results in very high joint rates near the points C and D while all of the other repeatable inverses are comparable to the performance obtained when using the pseudoinverse.

the augmented Jacobian is ill-conditioned, indicating proximity to an algorithmic singularity. It is this very behavior that makes the pure NUSAM technique unsatisfactory despite its computational advantages. However, using NUSAM as a precursor to the NORCS optimization results in the combined inverse which results in performance that compares more favorably with that of the pseudoinverse. In fact, a direct comparison of the combined inverse with that of the pure NORCS optimization over the entire basis $\mathcal{B}_5^l$ shows that the combined technique approaches optimal performance at a fraction of the computational expense. Finally, note that the use of a truncated basis for the optimization is justified by directly comparing the NORCS optimization with that of the optimal repeatable inverse over the infinite basis $\mathcal{B}_\infty$.

6. Conclusion

This work discusses techniques that make it practical to calculate repeatable generalized inverses which are close to some arbitrary desired generalized inverse. Two different types of optimizations are discussed. The first minimizes the integral norm of the difference between the repeatable inverse and the desired inverse

over a subset Ω. This directly solves the desired problem but the algorithm is computationally intractable for all but the simplest manipulators due to the high dimension of the search space. The second technique attempts to maintain the characteristics of the desired inverse by approximating its null vector. While this algorithm is relatively computationally efficient, it suffers from a poorer approximation of the desired inverse, primarily due to the effects of algorithmic singularities. While neither of these techniques is practical by itself, it has been shown that information gleaned from the null-space approximation technique can be used to guide the first technique in a lower-dimensional search space. This results in a computationally efficient approach for determining nearly optimal repeatable inverses that can approximate the properties of any given desired generalized inverse-control strategy.

Acknowledgements

This work was supported by Sandia National Laboratories under contract number 18-4379B. Additional support was provided by the NEC Corporation and the TRW Foundation.

Appendix

PROPOSITION. *Let M be an $N \times N$ real symmetric positive semi-definite matrix. Suppose $\mathbf{a} = M\mathbf{b}$. A solution of the constrained optimization problem*

$$\text{maximize } \mathbf{a}^T\mathbf{a}$$
$$\text{subject to } \mathbf{b}^T M\mathbf{b} = 1$$

is obtained when $\mathbf{b}$ is an appropriately scaled multiple of the singular vector associated with the largest singular value of M.

Proof. First, note that $\mathbf{a}^T\mathbf{a} = \mathbf{b}^T M^2\mathbf{b}$. Suppose the rank of M is r. Since M is a real symmetric positive semi-definite matrix, its singular value decomposition is USU^T where U is orthogonal and $S = \text{diag}(\sigma_1, \sigma_2, \ldots, \sigma_r, 0, \ldots, 0)$ with $\sigma_1 \geqslant \sigma_2 \geqslant \cdots \geqslant \sigma_r > 0$. Any vector $\mathbf{b}$ can be written as

$$\mathbf{b} = \alpha_1\mathbf{u}_1 + \alpha_2\mathbf{u}_2 + \cdots + \alpha_N\mathbf{u}_N \tag{A1}$$

where $\mathbf{u}_i$ is the ith column of U. Let

$$\mathbf{b}_1 = \alpha_1\mathbf{u}_1 + \alpha_2\mathbf{u}_2 + \cdots + \alpha_r\mathbf{u}_r. \tag{A2}$$

It is easy to verify that $\mathbf{b}_1^T M^2\mathbf{b}_1 = \mathbf{b}^T M^2\mathbf{b}$ and $\mathbf{b}_1^T M\mathbf{b}_1 = \mathbf{b}^T M\mathbf{b}$ so that one only needs to check vectors of the form (A2). Such vectors are given by $U_1\mathbf{w}$ where $U_1 = [\mathbf{u}_1, \mathbf{u}_2 \cdots \mathbf{u}_r]$ and $\mathbf{w}$ is an r-vector. The problem then becomes to

maximize $\mathbf{w}^T U_1^T M^2 U_1 \mathbf{w}$ subject to $\mathbf{w}^T U_1^T M U_1 \mathbf{w} = 1$ which is now rewritten as

$$\text{maximize } \mathbf{w}^T S_1^2 \mathbf{w}$$
$$\text{subject to } \mathbf{w}^T S_1 \mathbf{w} = 1$$

where $S_1 = \text{diag}(\sigma_1, \sigma_2, \ldots, \sigma_r)$. Applying the method of Lagrange multipliers

$$\frac{\partial}{\partial \mathbf{w}} \left[\mathbf{w}^T S_1^2 \mathbf{w} + \lambda \left(\mathbf{w}^T S_1 \mathbf{w} - 1 \right) \right] = 0 \tag{A3}$$

one finds that the optimal $\mathbf{w}$ satisfies $S_1^2 \mathbf{w} = -\lambda S_1 \mathbf{w}$. Since S_1 is invertible, $S_1 \mathbf{w} = -\lambda \mathbf{w}$. Thus the optimal $\mathbf{w}$ is an eigenvector of the diagonal matrix S_1. Suppose that the eigenvalue is c. Then $\mathbf{w}^T S_1^2 \mathbf{w} = c \mathbf{w}^T S_1 \mathbf{w} = c$, which implies that the maximum is given by choosing the largest singular value σ_1. This corresponds to choosing $\mathbf{b} = \mathbf{u}_1$.

References

1. Anderson, K. and Angeles, J.: Kinematic inversion of robotic manipulators in the presence of redundancies, *Int. J. Robotics Res.* **8**(6) (1989), 80–97.
2. Baillieul, J.: Kinematic programming alternatives for redundant manipulators, in *Proc. IEEE Int. Conf. Robotics Automat.*, St. Louis, MO, March 25–28, 1985, pp. 722–728.
3. Baker, D. R. and Wampler, C. W., II: On the inverse kinematics of redundant manipulators, *Int. J. Robotics Res.* **7**(2) (1988), 3–21.
4. Chiacchio, P., Chiaverini, S., Sciavicco, L. and Siciliano, B.: Closed-loop inverse kinematics schemes for constrained redundant manipulators with task space augmentation and task priority strategy, *Int. J. Robotics Res.* **10**(4) (1991), 410–425.
5. Colbaugh, R. and Glass, K.: On controlling robots with redundancy, *Robotics and Computer Integrated Manufacturing* **9**(2) (1992), 121–135.
6. Egeland, O.: Task-space tracking with redundant manipulators, *IEEE J. Robotics Automat.* **RA-3**(5) (1987), 471–475.
7. Klein, C. A. and Huang, C. H.: Review of pseudoinverse control for use with kinematically redundant manipulators, *IEEE Trans. Syst., Man Cyber.* **SMC-13**(3) (1983), 245–250.
8. Podhorodeski, R. P., Goldenberg, A. A. and Fenton, R. G.: Resolving redundant manipulator joint rates and identifying special arm configurations using Jacobian null-space bases, *IEEE Trans. Robotics Automat.* **7**(5) (1991), 607–618.
9. Roberts, R. G. and Maciejewski, A. A.: Nearest optimal repeatable control strategies for kinematically redundant manipulators, *IEEE Trans. Robotics Automat.* **8**(3) (1992), 327–337.
10. Roberts, R. G. and Maciejewski, A. A.: Repeatable generalized inverse control strategies for kinematically redundant manipulators, *IEEE Trans. Automat. Contr.* **38**(5) (1993), 689–699.
11. Seraji, H.: Configuration control of redundant manipulators: Theory and implementation, *IEEE Trans. Robotics Automat.* **5**(4) (1989), 472–490.
12. Shamir, T.: Remarks on some dynamical problems of controlling redundant manipulators, *IEEE Trans. Automat. Contr.* **35**(3) (1990), 341–344.
13. Shamir, T. and Yomdin, Y.: Repeatability of redundant manipulators: Mathematical solution of the problem, *IEEE Trans. Automat. Contr.* **33**(11) (1988), 1004–1009.

Journal of Intelligent and Robotic Systems **14**: 131–132, 1995

Calendar of Events

August 22–24, 1995
BICSC '95: 3rd Beijing Intl. Conf. on System Simulation and Scientific Computing. *Location*: Beijing, P.R. China. *Contact*: Prof. Zhang, Minglian, Chinese Association for System Simulation (CASS), 37, Xueyuan LU (College Road), Beijing 100083, P.R. China. Tel. 01–2026677–5477, 01–2026 677–4471, Fax: 86–1–201 5347, Telex: 222 [illegible] BUAA CN.

August 28–30, 1995
IMACS European Simul. Meeting on Simulation Tools and Applications. *Location*: Gyer, Hungary. *Contact*: IMACS Europ. Simul. Meeting, c/o Prof. Dr. A. Javor Scientific Society of Measurement and Automation, H-1372 Budapest, P.O. Box 451 Hungary. Fax: +36–1–1531406, e-mail: h7024vig@ella.hu

September 11–13, 1995
ICAM'95: Intl. Conf. on Advanced Manufacturing. *Location*: Sunderland, U.K. *Contact*: ICAM'95 Secretary, The Industry Center, The University of Sunderland, Hylton Riverside West, Wessington Way, Sunderland SR53XB, U.K., Tel.: +44–191–515 2666 Fax: +44–191–515–2669

September 12–14, 1995
Ethnicity & Nationalism in the New Europe Conf. *Location*: Univ. of Lancashire, U.K. *Contact*: Dr. Christopher Williams or Dr. Thanasis Sfikas, University of Central Lancashire, Dept. of European Studies, Harris Building, Corporation Street, Preston PR12HE, U.K., Tel.: (01772) 893920, Fax: (01772) 892919

September 18–22, 1995
ISATA'95: 28th Intl. Symp. on Automotive Technology and Automation: Manufacturing and Transportation. *Location*: Stuttgart, Germany. *Contact*: The ISATA'95 Secretariat 42, Lloyd Park Avenue, Croydon CR05SB, England, Tel.: +44–181–6813069, Fax: +44–181–6861490, e-mail: 100270.1263@compuserve.com

September 19–20, 1995
DARS'95: IFAC Workshop on Human-Oriented Design of Advanced Robotic Systems. *Location*: Vienna, Austria. *Contact*: IFAC-DARS'95, Institute for Handling Devices & Robotics (E318), University of Technology, Florgasse 7A, A-1040 Vienna, Tel.: +43–1–504 1835, Fax: +43–1–504 18359, e-mail: dars@ihrt1.ihrt.tuwien.ac.at

September 25–28, 1995
IFAC Symp. on Automated Systems Based on Human Skills – 'Joint Design of Technology and Organization'. *Location*: Berlin, Germany. *Contact*: VDI/VDE GMA, Gisa Recke Strasse 84, D-40239 Dusseldorf, Germany. Fax: +49–211–6214–161